

Conformation and Aggregation of Proline Esters and Their Aromatic Homologs: Pyramidal vs. Planar RR'N-H in Hydrogen Bonds

By Susanne Hesse and Martin A. Suhm*

Institut für Physikalische Chemie, Universität Göttingen, Tammannstr. 6, D-37077 Göttingen

Dedicated to Prof. Dr. Heinz-Georg Wagner on the occasion of his 80th birthday

(Received October 27, 2008; accepted March 8, 2009)

Proline Esters / Pyramidal RR'N-H / Planar RR'N-H / Hydrogen Bonds

The conformations of proline esters are investigated by infrared spectroscopy in supersonic slit jet expansions. Two easily convertible puckering variants of the pyrrolidine ring with intramolecular N-H...O contacts are shown to be particularly stable. The aggregation tendency of proline esters via intermolecular N-H...O hydrogen bonds is remarkably weak. IR differences between enantiopure and racemic dimers are difficult to quantify. Dehydrogenation of the pyrrolidine ring to pyrrole leads to a stable planar carboxylic ester conformation. Its aggregation tendency is pronounced due to the planar hybridization of the nitrogen atom and leads to a symmetric, β sheet-like dimer with strongly red-shifting hydrogen bonds. The spectroscopic observations underscore the differences between intermolecular interactions of N-terminal and peptide-bound amino acids in peptide chains.

1. Introduction

N-H bonds show wide property variations, ranging from the reactive N-H radical [1,2] to the biologically relevant hydrogen bond donors $N_{\text{py}}\text{-H}$ and $N_{\text{pl}}\text{-H}$, where the indices py and pl stand for a pyramidal or planar three-fold coordination of the N-atom. The natural coordination is pyramidal (sp^3 -hybridized), as found in ammonia, with the nitrogen lone electron pair occupying the opposite side of the pyramid. In this case, the in-plane arrangement of the three substituents only represents a transition state for umbrella inversion. If one or two of the nitrogen

* Corresponding author. E-mail: msuhm@gwdg.de

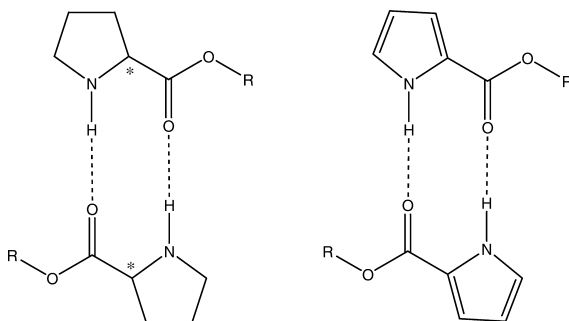


Fig. 1. Proline esters (asterisks mark the stereocenter) and pyrrole carboxylates in their syn form together with their symmetric dimerization options.

substituent bonds acquire partial double bond character, the attached H atom may join the plane which they define with the N-atom in what is commonly designated sp^2 hybridization. This is often the case for amides $RNH(C=O)R'$, where the N-C bond develops partial double bond character by resonance with the adjacent C=O bond. It is also the case in aromatic heterocycles such as pyrrole. In peptides and proteins, the N-H bonds of internal amino acids are sp^2 -hybridized, whereas the N-terminal amino group is sp^3 -hybridized, independent on whether it is protonated in the aqueous zwitterion or neutral in a less polar environment. N-H groups play an essential role in the supramolecular organization of peptides and their homologs [3].

Here, we wish to investigate the impact of N-H hybridization on the hydrogen bond aggregation tendency of simple peptide models by infrared spectroscopy. As a model for terminal amine groups, we choose proline esters (Fig. 1, left). Proline avoids the complication of intramolecular NH_2 oscillator coupling and therefore promises to be a dynamically simple N-terminal amino acid prototype. The OR ester group blocks the amino acid from zwitterionization and models the peptide backbone without introducing another nitrogen atom [4]. In contrast to aromatic amino acid esters [5], esters of proline are not accessible to selective UV double resonance techniques. In contrast to charged amino acids, sensitive ion trap techniques are not applicable [6]. Instead, the supersonic jet expansion has to be coupled to FTIR spectroscopy [7]. The unprotected amino acid proline is also accessible to gas phase FTIR spectroscopy [8], but currently only at elevated temperatures. Proline itself plays a special role in peptide conformations [9], which is related to its restricted flexibility and possibly also to its capability to switch on C-H \cdots O hydrogen bonds by ring puckering [10]. Furthermore, it is a key player in organocatalysis [11].

As a model for an sp^2 N-H group, we choose pyrrole carboxylates, which only differ from the proline esters by the aromaticity of the heterocycle. This in turn enforces planarity at the nitrogen (Fig. 1, right) and leads to two conformations [12] separated by a high barrier [13]. The alternative to introduce sp^2 hy-

bridization via acetylation [4] would remove the N-H donor in the case of proline. Specifically, we have studied methyl 1H-pyrrole-2-carboxylate (MPC), a compound which has been investigated before by IR spectroscopy and harmonic force field analysis at Hartree-Fock [14] and density functional [13] level, including also its dimer at HF/6-311+G* level [15] and suggesting that the solid is composed of dimers as well. The MPC dimer motif has also been used in crystal engineering [16]. These studies have focussed on condensed phases, where complications due to several conformations and possibly Fermi resonances [17] were discussed. We present low temperature supersonic jet data, which turn out to provide a very simple spectroscopic signature. It is rather similar to that of the related pyrrole-2-carboxaldehyde [18]. By capturing the essentials in this way, we hope to identify differences in aggregation and spectral signature between the two types of N-H bonds in the presence of carboxyl groups, which represent a classical biological hydrogen bond acceptor.

This study is organized in the following way. After an outline of the experimental details, the experimental spectra of proline esters are presented and discussed in section 3.1. Quantum-chemical calculations are used in section 3.2 to rationalize the experimental findings in terms of monomer conformations, dimer and trimer structures. Section 3.3 discusses the more straightforward pyrrole carboxylate case. The results are summarized in section 4 with emphasis on the characteristic differences between the two compound classes.

2. Experimental

Proline methyl ester hydrochloride was synthesized from proline (L-Proline: 99 %, Alfa Aesar; DL-Proline: 99 % ABCR) according to the method of Elliott et al. [19]. The hydrochloride salt was subsequently dissolved in water and mixed with one equivalent of K_2CO_3 . The mixture was extracted with dichloromethane. Another equivalent of K_2CO_3 in water was added and the mixture was once more extracted with dichloromethane. The dichloromethane was removed under vacuum, yielding 53 % of proline methyl ester as a clear liquid. Proline ethyl ester was synthesized according to the method of Federsel et al. [20] and yielded 91 % of the ester as a yellow oil. Neutral amino acid esters are somewhat more difficult to handle than their protonated forms [21]. The ethyl ester is more stable with respect to polymerization and was therefore investigated more extensively than the methyl ester. Due to the inherent polymerization tendency and low volatility of the amino acid esters, all reported gas phase concentrations are approximate. However, their relative size helps in assessing the clustering tendency and other trends. Methyl-pyrrolicarboxylate (MPC, 97 %, Aldrich) was used as supplied.

The compounds were mixed with a carrier gas (99.996% He and 99.998% Ar, Air Liquide) by flowing the gas through a thermostatted saturator containing the solid or liquid sample. Due to the low volatility of the compounds, residual

solvent and water traces could be removed quickly. About 2 mol s^{-1} of the gas mixture were dumped into a large vacuum chamber through a $600 \text{ mm} \times 0.2 \text{ mm}$ slit nozzle (*fine*, but *lengthy*, abbreviated *filet*) by opening six magnetic valves (Parker) for 135 ms [22]. In the adiabatic expansion zone directly after the slit nozzle, the molecules entrained in the gas pulse cool and aggregate quickly. In the case of Ar, the rare gas atoms may also condense on the molecules and aggregates [7]. A $\approx 15 \text{ mm} \times 15 \text{ mm}$ cross section of the long expansion zone was probed by the mildly focussed and recollimated IR beam of an Equinox 55 FTIR instrument equipped with a KBr or CaF_2 beamsplitter and suitable optical filters, scanned at 80 kHz to provide a spectral resolution of 2 cm^{-1} within 100 ms. The attenuation of the modulated IR beam caused by the pulsed gas absorption was monitored with an InSb or HgCdTe photon detector and referenced against the IR spectrum prior to the gas pulse. In this way, transient natural absorbances of less than 10^{-4} could be routinely detected.

3. Results and discussion

3.1 Experimental Proline Ester Spectra

Fig. 2 shows the gas phase spectrum of the ethyl ester of L-proline (trace a). It features a relatively strong band peaking at 3375 cm^{-1} with several shoulders to lower wavenumber, indicating a range of coexisting isomers. At 3482 cm^{-1} and thus somewhat too high for an isolated N-H stretching vibration, a moderately strong band is observed. Comparison of this band to the fundamental C=O stretching spectrum multiplied by 2 on the wavenumber axis (insert (a')) suggests a C=O stretching overtone origin. Such an overtone would be expected to have a small negative anharmonicity, consistent with the observed red-shift between experiment and harmonic prediction. The resulting diatomic C=O anharmonicity constant $\omega_e x_e = 11 \text{ cm}^{-1}$ falls in a reasonable range [23,24]. The overtone intensity is reduced by two orders of magnitude compared to the C=O fundamental. Therefore, no Fermi resonance intensity stealing from the N-H stretching mode has to be invoked to explain the overtone band in the IR spectrum. This is different in some sp^2 -hybridized cases [25].

In supersonic jet expansions (traces (b)-(d)), the broad N-H stretching fundamental separates into two, possibly three sharp bands marked A, B and B'. The band assigned to the C=O overtone is now lost or considerably reduced in intensity relative to the N-H stretching modes. Instead, weak unspecific bands appear to lower wavenumber (C) and are tentatively assigned to clusters of proline ethyl ester.

To investigate the latter two phenomena in more detail, we have also studied the proline methyl ester (Fig. 3). Again, the gas phase shows an isomer pattern in the N-H stretching range and an isolated C=O overtone candidate at 3492 cm^{-1} (Tab. 1). The shift of this band compared to the ethyl ester ($+10 \text{ cm}^{-1}$) correlates

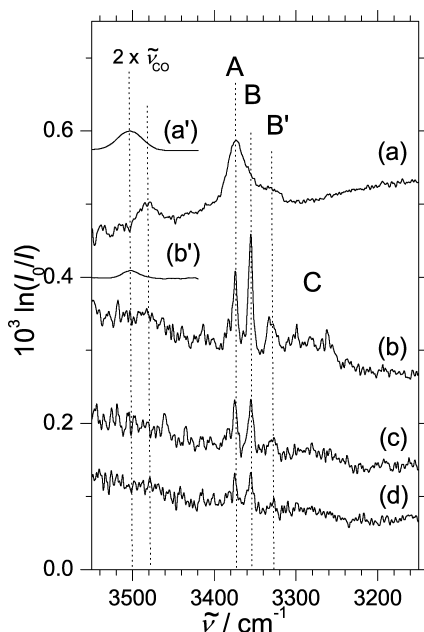
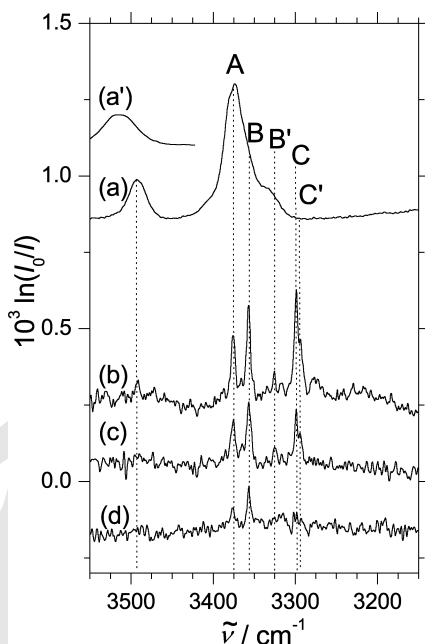


Fig. 2. N-H stretching region of the IR spectrum of enantiopure proline ethyl ester. (a) Gas phase after 10-fold compression, including an insert of the C=O fundamental on a $2\times$ stretched wavenumber scale after 3000-fold intensity compression (a'). (b) Jet spectrum of $< 0.01\%$ ester in He expanded at 1.3 bar, including an insert (b') obtained from the jet C=O fundamental by multiplying the wavenumber axis by 2 after 300-fold intensity compression. (c) Jet spectrum at reduced stagnation pressure (1.0 bar). (d) Further reduced stagnation pressure (0.7 bar).

with a shift of the C=O fundamental ($+7\text{ cm}^{-1}$) and further supports the overtone assignment. Similar to the observation in the ethyl ester, this overtone is attenuated by two orders of magnitude and it is consistent with an anharmonicity constant of 13 cm^{-1} of the isolated C=O stretching mode. Furthermore, the reduced inductive effect from ethyl to methyl explains the strengthening of the C=O bond. Indeed, MP2/6-311+G(d) calculations also predict harmonic C=O fundamental shifts by $+(4-5)\text{ cm}^{-1}$ when the ethyl group is replaced by a methyl group.

Table 1. Experimental N-H and C=O stretching wavenumbers $\tilde{\nu}_{\text{NH}}$ and $\tilde{\nu}_{\text{CO}}$ for proline esters in cm^{-1} .

	ethyl ester	methyl ester
$2\tilde{\nu}_{\text{CO}}$	3482	3492
$\tilde{\nu}_{\text{NH}}(\text{A})$	3375	3375
$\tilde{\nu}_{\text{NH}}(\text{B})$	3355	3357
$\tilde{\nu}_{\text{NH}}(\text{B}')$	3327	3326
$\tilde{\nu}_{\text{NH}}(\text{C}, \text{C}')$	3313–3245 (L) 3319–3246 (DL)	3299, 3294 (L) 3299, 3294 (DL)
$\tilde{\nu}_{\text{CO}}$	1752	1759

**Fig. 3.** N-H stretching region of the IR spectrum of enantiopure proline methyl ester. (a) Gas phase after 10-fold compression, including an insert (a') of the C=O fundamental on a $2\times$ stretched wavenumber scale. (b) Jet spectrum of about $\approx 0.03\%$ ester in He at 0.7 bar. (c) Reduced concentration ($\approx 0.02\%$ ester in He). (d) Reduced stagnation pressure (0.4 bar).

In contrast to the C=O overtone, the N-H stretching pattern of the proline esters is invariant to ester substitution (Tab. 1). In the jet, the A and B bands occur nearly at the same wavenumber, consistent with the remoteness of the N-H group relative to the ester alkyl group. Due to the somewhat higher vapor pressure of the methyl ester, cluster bands (C) are now more pronounced and peak at 3299 cm^{-1} . Again, the overtone band is at best weakly indicated in the

cold jet spectra, quite in contrast to the N-H stretching bands. Two effects must be invoked to explain this consistent lack of C=O-overtone visibility in the jet spectra. In contrast to N-H bands, the C=O bands may be broader, either intrinsically or due to the overlap of several isomer contributions. This is partially the case, as insert (b') in Fig. 2 shows. It represents the wavenumber-doubled jet spectrum of the C=O fundamental, which shifts slightly (2 cm^{-1}) to lower wavenumber with increased cluster extent, but remains otherwise unstructured and broad. However, some temperature dependence of the N-H fundamental to C=O overtone intensity ratio must also be invoked to explain the weak jet signal in the C=O overtone region. It is well known that hydrogen bonding tends to enhance hydride stretching fundamentals, whereas it does not enhance and may even attenuate overtone transitions [26]. Thus, our jet spectra provide indirect evidence for intramolecular hydrogen bonding in proline esters. We note that in liquid state spectra of the ethyl ester (not shown), the overtone is also absent, consistent with our interpretation.

A common feature of the N-H stretching jet spectra of both proline esters is that the A/B intensity ratio depends on the expansion conditions. This could either be due to an underlying cluster absorption in the range of the B band or due to a difference in relative stability of the A and B conformations. In the latter, more likely case, the A and B' conformations appear to be less stable than the B conformation. This stability trend within the jet spectra continues the trend from the room temperature gas phase spectrum, where A was the dominant conformation. Either A is entropically favored over B, or else the B intensity profits more from a weak internal hydrogen bond, which is formed at lower temperatures.

To distinguish among these two explanations, an Ar relaxation study was carried out for the proline ethyl ester. In this experiment, a progressive amount of He carrier gas is replaced by Ar, a more efficient collisional relaxation partner. If too much Ar is added, it starts to condense on the molecules, leading to matrix-like spectral shifts of the bands. Fig. 4 shows the results of adding up to 4 % Ar. One can clearly see that band A is depleted in favor of B upon the addition of 1.5 % Ar. This strongly favors the hypothesis that the red-shifted band B belongs to the global minimum structure of proline esters. At 4 % Ar, a weak red-shifted band emerges. It may be due to proline ester clusters, in analogy to band C in Fig. 3 for the more volatile methyl ester. The size of the shift is too large to be due to Ar-coated monomers.

To exclude the remote possibility that the A and B bands have a cluster origin, rather than being due to monomers, we have studied an expansion of racemic proline ethyl ester. This should not affect the monomer spectra, whereas some chirality recognition [27] might be expected in dimers and higher aggregates, because of the diastereomeric nature of the resulting units. As Fig. 5 and exact band positions show, there is no change in A and B within experimental error, whereas the cluster pattern C appears to differ somewhat from that in Fig. 2. Unfortunately, the spectral complexity and limited signal-to-noise ratio

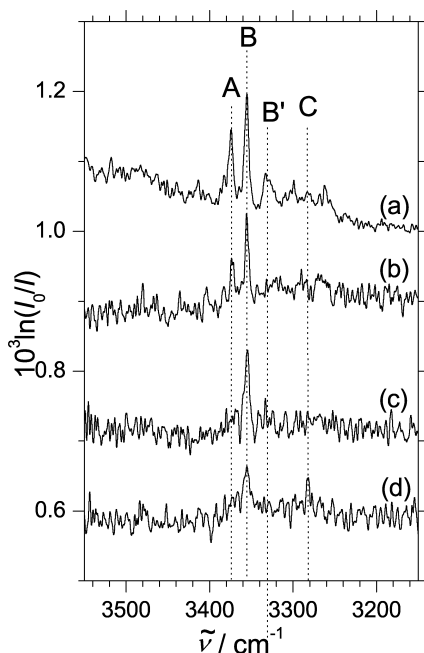


Fig. 4. N-H stretching region of the jet IR spectrum of $< 0.01\%$ proline ethyl ester in He as a function of Ar admixture at a stagnation pressure of 1.3 bar. (a) 0% Ar, (b) 1% Ar, (c) 1.5% Ar, (d) 4% Ar.

in this chemically labile system does not allow for a detailed experimental study of chirality recognition in proline ethyl ester dimers, at this stage.

For proline methyl ester, the vapor pressure is higher and the cluster tendency (reflected in the C bands) is more pronounced. Therefore, Fig. 6 compares spectra of enantiopure and racemic expansions of the methyl ester directly to each other. Even in the cluster signal range (C), differences in the band positions are negligible. The only difference is a significantly lower peak absorbance in the racemic case. However, it is difficult to quantify. Therefore, it must remain open whether the C band is mainly due to homochiral clusters, which are statistically reduced in the racemic experiment, or whether homochiral and heterochiral clusters have very similar spectra.

The main peak positions are provided in Tab. 1. The experimental findings may be summarized as follows: At low temperatures, proline esters occur in two conformations, which appear to be spectrally enhanced in the N-H stretching range by a weak intramolecular hydrogen bond. The conformation with the lower N-H stretching frequency is more stable and internal rotation within the ester group has little effect on the spectra. In contrast to the related lactates [28], signatures of cluster formation are quite unspecific with the exception of a possi-

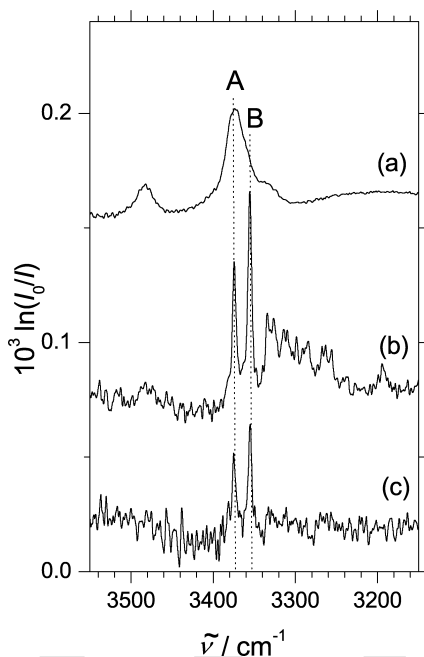


Fig. 5. N-H stretching region of the IR spectrum of racemic proline ethyl ester. (a) Gas phase after 20-fold intensity compression. (b) Jet spectrum of < 0.01% ester in He at 1.3 bar. (c) Reduced stagnation pressure (1.0 bar).

bly homochiral cluster, which shows up in relatively concentrated or cold expansions.

3.2 Quantum chemical calculations for proline esters

An important goal of the present study is to provide quantum chemistry with experimental benchmark data for simple prototype systems. Proline systems have been shown to offer challenging goals [29]. Here, we start with some medium level approaches obtained using the Gaussian program suite [30] to see how well they perform in reproducing the spectroscopic findings.

Tab. 2 summarizes relative energies of 8 conformations of proline methyl ester, which are shown in Fig. 7. They differ in ring puckering, torsion of the ester group and N-H orientation. These structures were obtained from a search involving 120 starting structures at a low level (HF/3-21+G) and confirmed to represent local minima at the following levels of approximation: HF/6-31+G(d), B3LYP/6-31+G(d), B3LYP/6-311++G(d,p), MP2/6-311+G(d). Only the latter three levels are included in Tab. 2. There are some reorderings of the relative

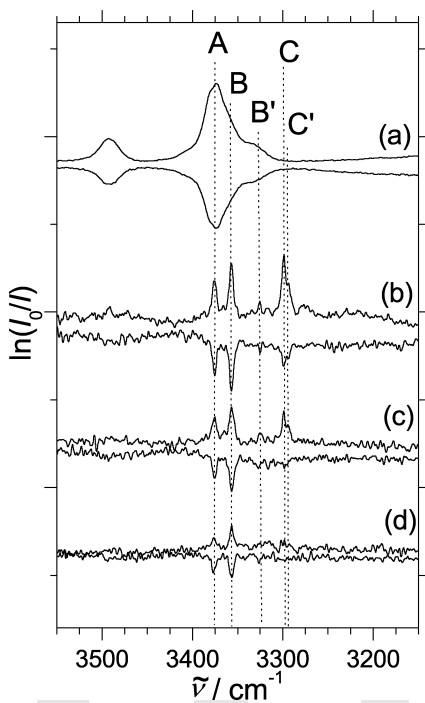


Fig. 6. Spectral comparison between enantiopure proline methyl ester (pointing up) and racemic proline methyl ester (pointing down) in (a) the gas phase and (b-d) under decreasing clustering conditions in the jet. The jet spectra are scaled to similar monomer peak absorbance B.

energy, but all calculations agree that there are only two favorable conformations within a window of 4 kJ mol^{-1} (VII, VIII). These two are thus candidates for the two observed N-H stretching bands. Both involve a close contact between the pyrrolidine N-H and the ester C=O group (224–240 pm), and they are the only ones to do so. Although the interaction involves a ring of only four heavy atoms, it appears to stabilize the conformation. In the next most stable conformations (I and VI), hydrogen bond contacts to the ester oxygen at similar distances are found. For proline ethyl ester, a very similar set of structures and energies was obtained.

The importance of the intramolecular N-H \cdots O=C contact is emphasized by the fact that the most stable ring conformation of the bare pyrrolidine without ester group differs from that of the proline esters [31]. Proline itself also differs in conformational preference inasmuch as an O-H \cdots N interaction can be realized in the unprotected amino acid [32]. This and its puckering variant indeed lead to the experimentally observed proline structures [9,29]. However, the next most stable proline structures correspond to the two preferred proline ester structures (VII and VIII), at least at sufficiently high levels of approximation, and have also

Table 2. Relative energies of 8 conformations of proline methyl ester in kJ mol^{-1} with (ΔE_c) and without (ΔE_0) inclusion of harmonic zero point energy. The conformations are ordered by decreasing MP2/6-311+G(d) energy ΔE_0 .

	B3LYP/6-31+G(d)		B3LYP/6-311++G(d,p)		MP2/6-311+G(d)	
	ΔE_c	ΔE_0	ΔE_c	ΔE_0	ΔE_c	ΔE_0
III	10.86	10.73	10.75	10.61	9.58	9.70
IV	10.59	10.38	10.78	10.33	9.33	9.62
II	8.34	8.40	8.11	8.13	8.26	8.35
V	6.78	6.38	6.86	6.47	6.73	6.34
VI	8.41	7.87	8.02	7.56	5.46	5.11
I	7.31	6.80	6.42	6.41	5.20	5.10
VII	0.73	1.23	0.51	0.71	0.90	1.06
VIII	0.00	0.00	0.00	0.00	0.00	0.00

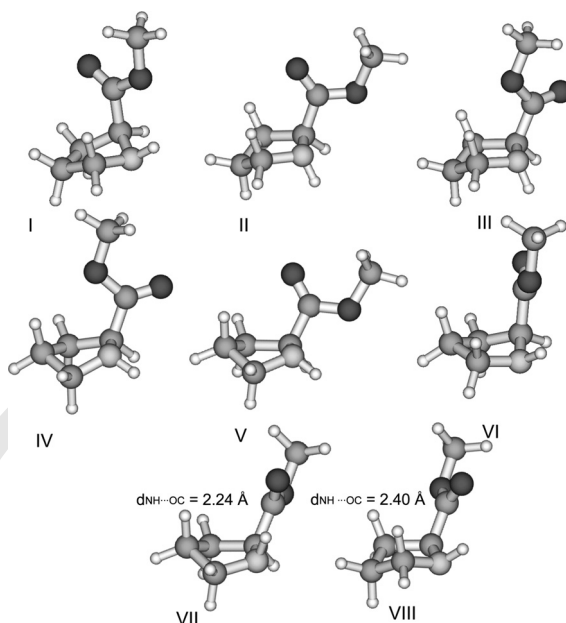


Fig. 7. Eight conformations of proline methyl ester calculated at MP2/6-311+G(d) level.

been observed in cryogenic matrices [29]. Analogous structures are preferred in protonated and deprotonated proline [33] and the N-H \cdots O=C bond motif also dominates in other neutral amino acids in the gas phase [29]. Therefore, the following discussion can consistently focus on the two N-H \cdots O=C-stabilized structures VII and VIII.

Tab. 3 summarizes the spectral predictions for the methyl ester obtained at various harmonic levels of approximation. They are qualitatively robust in pre-

Table 3. N-H and C=O stretching wavenumbers $\tilde{\nu}$ in cm^{-1} and band strengths I in km mol^{-1} of the two most stable structures of proline methyl ester obtained at various harmonic levels of approximation as well as wavenumber differences between conformers VIII and VII.

	B3LYP/6-31+G(d)	B3LYP/6-311++G(d,p)	MP2/6-311+G(d)
$\tilde{\nu}_{\text{NH}}(\text{VII}) / \text{cm}^{-1}$	3495	3518	3551
$\Delta\tilde{\nu}_{\text{NH}}(\text{VIII-VII}) / \text{cm}^{-1}$	37	27	13
$I_{\text{NH}}(\text{VII}) / \text{km mol}^{-1}$	19	25	21
$I_{\text{NH}}(\text{VIII}) / \text{km mol}^{-1}$	15	18	11
$\tilde{\nu}_{\text{CO}}(\text{VII}) / \text{cm}^{-1}$	1788	1780	1782
$\Delta\tilde{\nu}_{\text{CO}}(\text{VIII-VII}) / \text{cm}^{-1}$	-2	0	1
$I_{\text{CO}}(\text{VII}) / \text{km mol}^{-1}$	224	227	187
$I_{\text{CO}}(\text{VIII}) / \text{km mol}^{-1}$	233	237	195

dicting two closely spaced N-H stretching bands, with structure VIII being slightly less visible and shifted to a higher wavenumber. We note that other conformers carry at least a factor of two less oscillator strength – another evidence for the stabilizing N-H...O=C hydrogen bond in conformers VII and VIII. Furthermore, all calculations predict the C=O stretching bands within the spectral resolution for monomer VII and VIII, fully consistent with the experimentally observed single C=O stretching fundamental and overtone. The only discrepancy between theory and experiment is found for the relative sequence of VII and VIII. Experiment is unambiguous in locating the more stable conformation at the lower N-H stretching wavenumber, whereas Tab. 2 and 3 together suggest the opposite. A sign switch in the $\approx 20 \text{ cm}^{-1}$ wavenumber difference appears unlikely, as any anharmonic contributions are likely to cancel among the two conformations, to a large extent. However, energy differences on the order of 1 kJ mol^{-1} are less robust with respect to higher levels of approximation. Indeed, already a single point MP2/aug-cc-pVTZ calculation at the MP2/6-311+G(d) structure reverses the energy sequence, so that structure VII is now 0.7 kJ mol^{-1} more stable than VIII. This is also consistent with the shorter N-H...O=C hydrogen bond in structure VII (224 pm) compared to VIII (240 pm). Structure optimization at the MP2/aug-cc-pVTZ level increases the energy difference to 0.9 kJ mol^{-1} . Thus, only at MP2/aug-cc-pVTZ level (and incidentally also at HF/3-21+G level) is the energy difference between the two hydrogen bonded puckering isomers of proline methyl ester predicted correctly. With this assignment, the experimental VIII-VII N-H stretching wavenumber shift of 19 cm^{-1} is seen to be reproduced reasonably well (Tab. 3) by moderately sized basis set MP2 and B3LYP calculations. Considering that isomer VIII is a somewhat weaker absorber (Tab. 3), the two conformers are formed in similar abundance in the He expansion (Fig. 3). Only by adding Ar to the expansion, isomer VIII is converted to isomer VII.

To exclude a coincidental agreement, the same analysis was carried out for the ethyl ester of proline. After checking that the influence of gauche/trans

Table 4. N-H stretching wavenumbers $\tilde{\nu}_{\text{NH}}$ in cm^{-1} and relative band strengths I in km mol^{-1} of the two most stable structures of proline ethyl ester obtained at various harmonic levels of approximation. The ester group is trans relative to the O-C bond.

	B3LYP/6-31+G(d)	B3LYP/6-311++G(d,p)	MP2/6-311+G(d)
$\tilde{\nu}_{\text{NH}}(\text{VII}) / \text{cm}^{-1}$	3490	3520	3551
$\Delta\tilde{\nu}_{\text{NH}}(\text{VIII-VII}) / \text{cm}^{-1}$	41	24	12
$I_{\text{NH}}(\text{VII}) / \text{km mol}^{-1}$	19	27	21
$I_{\text{NH}}(\text{VIII}) / \text{km mol}^{-1}$	16	19	11
$\tilde{\nu}_{\text{CO}}(\text{VII}) / \text{cm}^{-1}$	1783	1775	1777
$\Delta\tilde{\nu}_{\text{CO}}(\text{VIII-VII}) / \text{cm}^{-1}$	-2	0	1
$I_{\text{CO}}(\text{VII}) / \text{km mol}^{-1}$	231	233	193
$I_{\text{CO}}(\text{VIII}) / \text{km mol}^{-1}$	239	244	201

isomerism in the ethyl group is minor ($\approx 0.3\text{--}1.0 \text{ kJ mol}^{-1}$ in the energy difference, $\approx 1\text{--}3 \text{ cm}^{-1}$ in the C=O stretching wavenumber, $\approx 0\text{--}5 \text{ cm}^{-1}$ in the N-H stretching wavenumber), the systematic study was restricted to the ethyl trans conformation. The energetical results typically agree within 0.5 kJ mol^{-1} or 10%. In particular, the qualitative energy sequence persists. Tab. 4 shows that the spectral predictions also agree with those of the methyl ester, in line with the experimental findings.

After having explained the experimental monomer observations, we can turn to an explanation of the experimental low clustering propensity of proline esters. For this purpose, several dimer calculations were carried out at the B3LYP/6-311++G(d,p) level. As expected, dimers built from conformations other than VII and VIII are not found to be competitive. Therefore we can concentrate on the conformations generated by these two isomers. Fig. 8 gives a survey over some stable structures obtained, including homochiral (SS) and heterochiral (SR) pairs. They may be classified into dimers with two intermolecular N-H...O=C hydrogen bonds and dimers in which the N-H group of one monomer inserts into the intramolecular contact of the other, leading to a N-H...N-H...O=C topology (marked with an i in the name).

Two remarkable findings may be extracted from the B3LYP data listed in Tab. 5. The first is that there are several stable dimer structures predicted within about 2 kJ/mol of the global minimum structure, likely to be competitively populated in a supersonic jet expansion. There seems to be little energy difference between inserted and symmetric hydrogen bond topologies and a rather erratic behavior with respect to chirality recognition. The second remarkable finding is that the binding energies themselves are surprisingly small, on the order of 5 kJ/mol per hydrogen bond at this level. This is comparable to the distortion energy which has to be invested into the monomers in order to make them ready for double intermolecular hydrogen bonding. If two hydrogen bond-like N-H...O=C contacts do not contribute more than 5 kJ mol^{-1} , each, dispersion interactions must play an important role and may even dominate the electro-

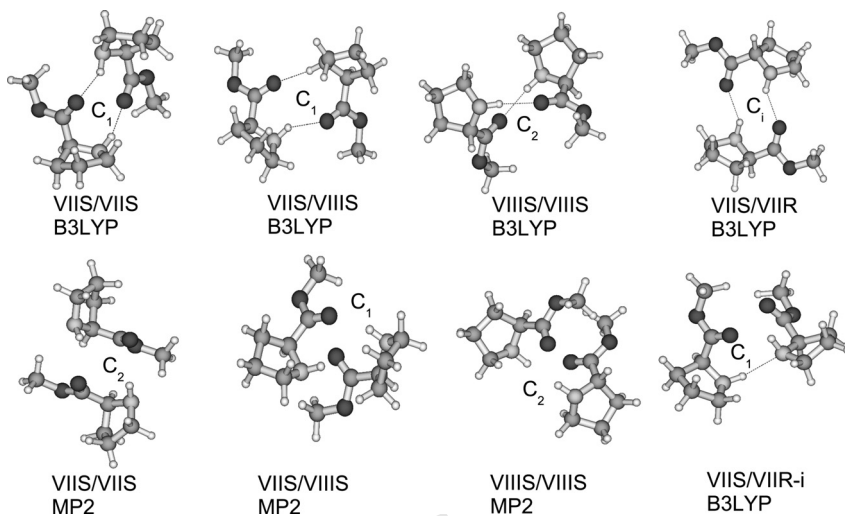


Fig. 8. Structures of selected homochiral and heterochiral proline methyl ester dimers at B3LYP/6-311++G(d,p) and MP2/6-311+G(d) level.

static component associated with hydrogen bonds. Thus, functionals such as B3LYP cannot be expected to provide an adequate description of the dimer energetics. Indeed, MP2 optimizations carried out for some of the structures (Tab. 5) reveal about four times larger binding energies and also some structural readjustments (see Fig. 8) which indicate the importance of dispersion interactions and weak hydrogen bond contacts involving C-H bonds, despite basis set superposition contributions.

In line with the weak electrostatic cohesion, B3LYP calculations also predict small and nonsystematic wavenumber shifts of the N-H oscillator and the C=O fundamental for the proline ester dimers. Nevertheless, the IR intensity enhancement of the N-H oscillator is quite significant, reaching up to an order of magnitude. Fig. 9 contains some spectral simulations of enantiopure proline methyl ester expansions, based on the assumption that isomers VII and VIII have equal abundance in the jet expansion and that each of the possible dimers has a relative abundance of 2 %, an upper limit for such a weakly complexing compound. Clearly, the simulated dimer N-H stretching spectra do not correlate with the observed cluster structures. Except for some inserted structures, they lack a systematic red-shift. This is also true for the harmonic predictions at MP2 level. Apparently, dimers are only present in trace amounts in the proline ester expansions.

Analogous simulations for the ethyl ester are shown in Fig. 10. The underlying dimer structures are similar to the ones found for the methyl ester. One cannot rule out contributions from such dimers to the broad red-shifted absorption fea-

Table 5. Comparison of different dimer and trimer structures of proline methyl ester in terms of their relative energies ΔE_c and ΔE_0 and dissociation energies D_c/n and D_0/n into the corresponding n fragments in kJ mol^{-1} .

	B3LYP/6-311++G(d,p)				MP2/6-311+G(d)		
	ΔE_c	ΔE_0	D_c/n	D_0/n	ΔE_c	D_c/n	D_0/n
Dimer							
VIIIS/VIIIS (C_2)	0.45	0.00	5.96	5.13	8.00	20.16	18.90
VIIIS/VIIIR (C_1)	0.47	0.81	6.21	5.08	-	-	-
VIIIS/VIIIR-i (C_1)	0.00	0.93	6.69	5.38	-	-	-
VIIIS/VIIIS (C_1)	0.45	0.99	6.21	4.99	5.72	21.75	-
VIIIS/VIIIR (C_1)	0.73	1.59	6.33	5.05	-	-	-
VIIIS/VIIIS-i (C_1)	0.93	1.77	6.23	4.95	7.78	21.17	-
VIIIS/VIIIS (C_1/C_2)	1.06	2.54	5.94	4.57	0.00	25.07	19.96
VIIIS/VIIIR (C_1)	5.01	4.11	3.68	3.07	-	-	-
Trimer							
VII/VII/VII A (C_3)	0.00	0.00	11.36	9.74	-	-	-
VII/VII/VII B (C_1)	3.22	4.68	10.29	8.18	-	-	-

tures, but specific assignments are beyond the quality of the spectra and the quantum chemical calculations at this stage.

The calculated B3LYP and MP2 dimer binding energies may be compared to approximate evaporation enthalpies of proline esters based on vapor pressure curves from literature data [34,35,36,37,38]. The evaporation enthalpy of the proline methyl ester may be estimated around 45 kJ mol^{-1} from these data. This is an order of magnitude more than the equivalent of one or two $\text{N-H}\cdots\text{O}=\text{C}$ hydrogen bonds and provides strong evidence for the dominance of non-directional, dispersion-like interactions or $\text{N-H}\cdots\text{N-H}$ interactions in these systems, which are not covered at B3LYP level. The evaporation enthalpy of the ethyl ester is 10 % higher, consistent with enhanced dispersion interactions. The MP2 dimer binding energies, which still contain considerable uncertainties due to basis set superposition and other incompleteness errors, are of the correct order of magnitude to explain cohesion in proline esters.

At this point it is worthwhile to analyze the cohesion energy of proline ester dimers by comparison to simple model dimers involving isolated functional groups. This is done in Tab. 6 for the complexes of dimethyl amine and methyl acetate. At B3LYP level, the isolated interactions are about twice as strong as the corresponding interactions in the proline ester dimer. This points at a competition between the intramolecular $\text{N-H}\cdots\text{O}=\text{C}$ contact, which is only present in the proline ester, and the intermolecular hydrogen bond. At MP2 level, this difference appears to vanish. More likely, it is compensated by additional dispersion forces in the larger unit. Comparison to the dimer of dimethyl amine shows that $\text{N-H}\cdots\text{N-H}$ hydrogen bonds are not more attractive in the dimer. Their strength is similar and there can only be one such bond in a dimer, possibly augmented by a $\text{N-H}\cdots\text{O}=\text{C}$ interaction.

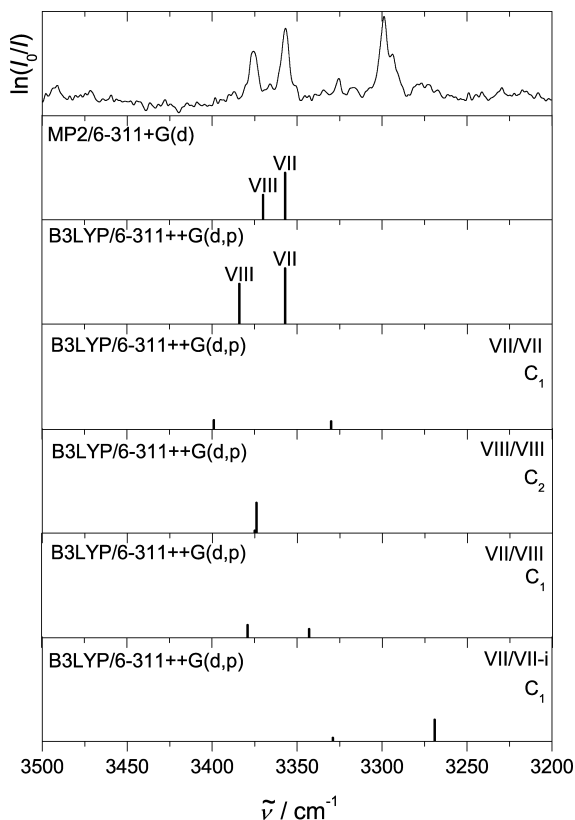


Fig. 9. Spectral simulations of enantiopure proline methyl ester expansions, matching the N-H stretching transitions of conformer VII to experiment and including several dimer structures.

The situation changes in larger clusters, where one N-H \cdots N-H bond per monomer can be realized. In addition, a sequence of N-H \cdots N-H \cdots N-H bonds can show signs of cooperativity, like in the analogous hydroxyester case [39]. This could explain both an enhanced stability and an enhanced red-shift. We have therefore started to explore structures for proline ester trimers in order to find a qualitative explanation for the cluster signature in the spectra. Tab. 5 contains results for a C_3 -symmetric cooperatively bound trimer involving mainly NH \cdots NH hydrogen bonds and a more complex structure without symmetry building on a dimer with secondary N-H \cdots N-H coordination (see Fig. 11). At B3LYP level, they are of comparable energy. The binding energy per hydrogen bond is nearly twice as high as in the dimers, but still low at B3LYP level. As Fig. 12 shows, the more stable trimer structure may account for parts of the cluster signal near 3300 cm^{-1} , but at the currently accessible level of calculation, this remains speculative.

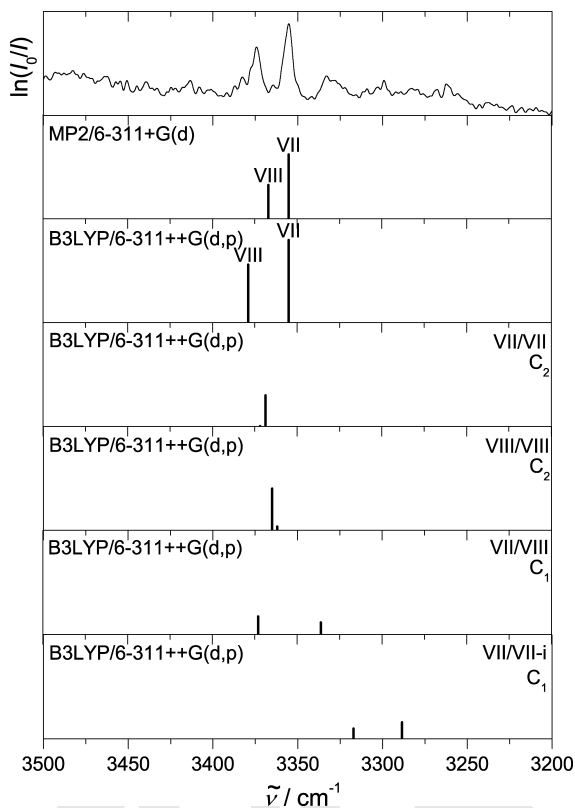


Fig. 10. Spectral simulations of enantiopure proline ethyl ester expansions, matching the N-H stretching transitions of conformer VII to experiment and including several dimer structures.

Table 6. Comparison of MPC, proline esters and a selection of small model dimers concerning the dissociation energies D_e/n and D_0/n per hydrogen bond in kJ mol^{-1} . If several structures are possible, the most stable one at the highest level of calculation is chosen.

dimer		B3LYP/6-311++G(d,p)		MP2/6-311+G(d)	
		D_e/n	D_0/n	D_e/n	D_0/n
dimethylamine/ methyl acetate	$\text{NH}_{sp}^3 \cdots \text{O}=\text{C}$	13	9	23	19
dimethylamine/ dimethylamine	$\text{NH}_{sp}^3 \cdots \text{NH}_{sp}^3$	13	9	24	21
proline ester/ proline ester	$\text{NH}_{sp}^3 \cdots \text{O}=\text{C}$	4-6	4-6	25	
formamide/ methyl acetate	$\text{NH}_{sp}^2 \cdots \text{O}=\text{C}$	30	24	37	32
MPC/MPC	$\text{NH}_{sp}^2 \cdots \text{O}=\text{C}$	25	23	30	

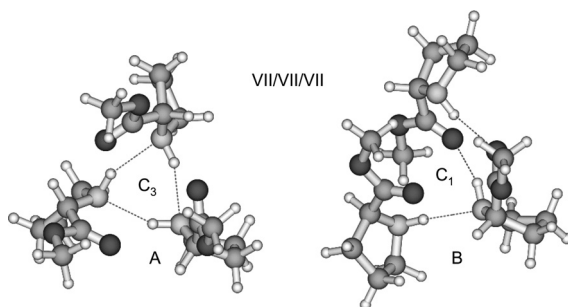


Fig. 11. Structures of two homochiral proline methyl ester trimers with different hydrogen bond topology at B3LYP/6-311++G(d,p) level.

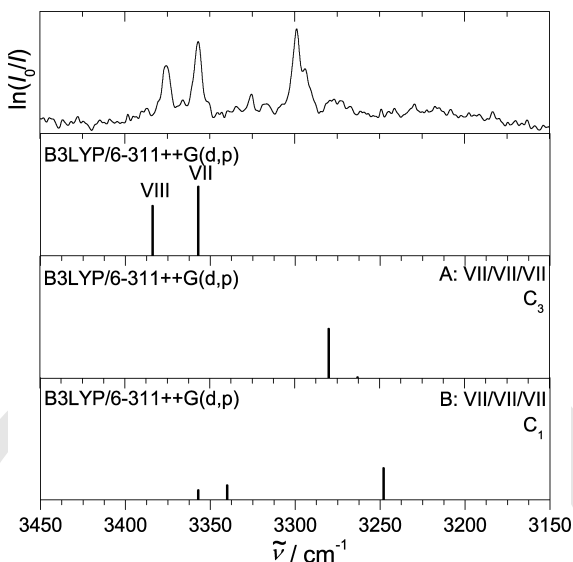


Fig. 12. Spectral simulations of enantiopure proline methyl ester expansions, matching the N-H stretching transitions of conformer VII to experiment and including two trimer structures. 2 % trimer abundance is assumed for each of the trimer structures.

In summary, neither the calculations nor the spectra indicate a high degree of directionality and selectivity in the aggregates of proline esters. Molecular recognition remains undifferentiated. The supersonic jet expansions are dominated by two monomer conformations which reflect ring puckering in combination with an intramolecular hydrogen bond-like contact. Enhancement of the cluster fraction in higher temperature nozzles is difficult in the case of proline esters, because of their limited thermal stability.

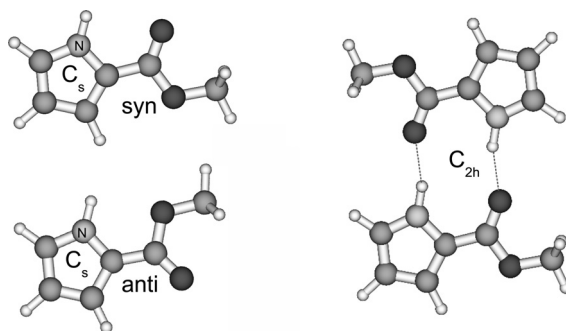


Fig. 13. Monomer conformations (syn and anti refer to the relative position of the N-H and C=O groups) and most stable dimer structure of MPC, calculated at B3LYP/6–311++G(d,p) level.

3.3 Pyrrole carboxylates

The two monomer conformations of MPC [13] and the most stable C_{2h} dimer structure are shown in Fig. 13. Investigation of other possible dimer structures shows that the next-lowest conformation is at least 20 kJ mol^{-1} less stable than the inversion-symmetric one shown in Fig. 13. Being a supersonic jet study, this work can thus focus on the C_{2h} symmetric structure. Its dissociation energy without zero-point energy correction D_e is predicted to be 49.3 kJ mol^{-1} at B3LYP/6–311++G(d,p) level and 60.5 kJ mol^{-1} at MP2/6–311+G(d) level. Inclusion of zero-point energy at the harmonic level of approximation only leads to a minor reduction in the B3LYP dissociation energy (45.0 kJ mol^{-1}). This corresponds to a sizeable hydrogen bond strength of $25\text{--}30 \text{ kJ mol}^{-1}$ for the aromatic N-H \cdots O=C hydrogen bond, quite in contrast to the aliphatic value in the proline ester case discussed before.

An analysis of these binding energies in terms of isolated building blocks, namely formamide [40] and methyl acetate [41], reveals that the two functional groups are largely decoupled in terms of their interaction strength (Tab. 6). Replacement of formamide by pyrrole [42] is likely to confirm this additivity on a coarse energy scale, whereas subtle spectroscopic differences are to be expected. These may reflect either through-bond conjugation [42] or through-space intramolecular interactions [17].

The energy difference between the two monomer conformations is predicted to be on the order of $4\text{--}5 \text{ kJ mol}^{-1}$ (see Tab. 7). This is in good agreement with earlier density functional results [13]. The barrier is very high [13] such that any thermally populated fraction of the higher-lying conformation [12] is expected to be frozen in the jet expansion.

Table 7. Isomerization energies for the transition from the most stable (syn) MPC structure to the less stable (anti) rotamer in kJ mol^{-1} excluding (E_c) and including (E_0) zero-point energy corrections.

level	E_c	E_0
B3LYP/6-31+G(d)	5.1	4.8
B3LYP/6-311++G(d,p)	4.5	4.2
MP2/6-311+G(d)	4.2	

Table 8. N-H stretching wavenumbers in cm^{-1} of the most stable monomer ($\tilde{\nu}_{\text{NH}}(\text{M})$) and dimer structure (Raman active $\tilde{\nu}_{\text{NH}}(\text{D}_{\text{Ra}})$, IR-active $\tilde{\nu}_{\text{NH}}(\text{D}_{\text{IR}})$) of MPC and band strengths I in km mol^{-1} obtained at various harmonic levels of approximation. The MP2 values are only of limited relevance, because the force field calculations reveal imaginary wavenumbers for M and D as a consequence of the small basis set [18].

	B3LYP/6-31+G(d)	B3LYP/6-311++G(d,p)	MP2/6-311+G(d)
$\tilde{\nu}_{\text{NH}}(\text{M}) / \text{cm}^{-1}$	3644	3645	3653
$I_{\text{NH}}(\text{M}) / \text{km mol}^{-1}$	91	100	96
$\Delta\tilde{\nu}_{\text{NH}}(\text{M}-\text{D}_{\text{Ra}}) / \text{cm}^{-1}$	175	200	135
$\Delta\tilde{\nu}_{\text{NH}}(\text{M}-\text{D}_{\text{IR}}) / \text{cm}^{-1}$	164	188	126
$I_{\text{NH}}(\text{D}_{\text{IR}}) / \text{km mol}^{-1}$	1887	1985	1656
$\tilde{\nu}_{\text{CO}}(\text{M}) / \text{cm}^{-1}$	1746	1740	1762
$I_{\text{CO}}(\text{M}) / \text{km mol}^{-1}$	413	420	330
$\Delta\tilde{\nu}_{\text{CO}}(\text{M}-\text{D}_{\text{Ra}}) / \text{cm}^{-1}$	29	32	12
$\Delta\tilde{\nu}_{\text{CO}}(\text{M}-\text{D}_{\text{IR}}) / \text{cm}^{-1}$	22	24	13
$I_{\text{CO}}(\text{D}_{\text{a}}) / \text{km mol}^{-1}$	1406	1447	1174

The IR predictions (Tab. 8) for the monomer and the dimer are correspondingly simple and straightforward. A moderately strong N-H stretching fundamental is predicted for the monomer. In the dimer, the N-H stretching modes are substantially shifted to lower wavenumber. Only the less shifted one carries IR intensity, which is enhanced over that of the monomer by more than an order of magnitude. The C=O stretching mode is much stronger in the monomer, but still gains intensity in the dimer. It is red-shifted by the hydrogen bond interaction in the dimer. There is quantitative disagreement between the B3LYP and MP2 dimerization shift predictions, as usual for such systems. Specifically, the MP2 shift is smaller than that at B3LYP level, although the hydrogen bond energy is higher. This is similar to the case of pyrrole-2-carboxaldehyde [18], where the MP2 force field predictions were shown to have serious deficiencies for medium-sized Pople basis sets. For the pyrrole-carboxylate we also find imaginary frequencies (one in the monomer and four in the dimer) but at least no unexpected blue shift in the MP2 calculations. Clearly, the B3LYP calculations are more in line with expectations for such a strongly hydrogen-bonded dimer.

With these predictions at hand, the experimental jet expansion spectra may be discussed. One should note that the volatility of MPC is close to the detection

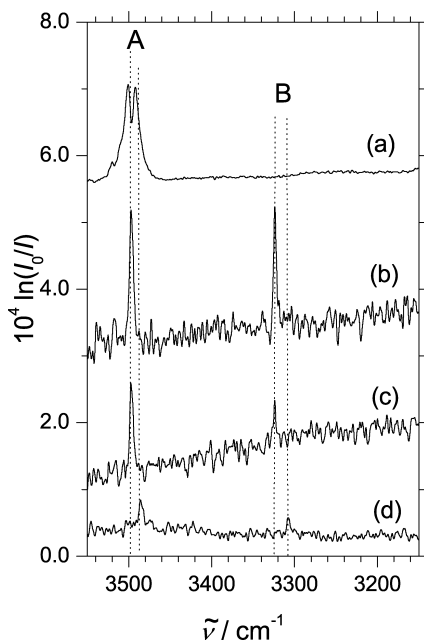


Fig. 14. N-H stretching region of the IR spectrum of methyl 1H-pyrrole-2-carboxylate. (a) Gas phase after 10-fold intensity compression. (b) Jet spectrum of $\leq 0.003\%$ MPC in He at 1.3 bar. (c) Reduced stagnation pressure (0.7 bar). (d) Jet spectrum of $\leq 0.003\%$ MPC in Ar at 0.7 bar.

limit of the room temperature filet-jet FTIR setup. Therefore, only the strongest bands can be observed.

Fig. 14 shows the N-H stretching range recorded in the room temperature gas phase (top trace) and compares it to a range of supersonic jet spectra. Within the $\approx 5:1$ signal-to-noise ratio, only a single monomer conformation is observed in the jet at 3497 cm^{-1} . This is consistent with a $\geq 4\text{ kJ mol}^{-1}$ energy penalty for the metastable conformation, i.e. with the theoretical predictions. A weak feature near 3517 cm^{-1} might be due to the second isomer, as theory [13] predicts a blue-shift of about 18 cm^{-1} . However, the band is too weak to be safely assigned. In an Ar expansion, the main band shifts to 3485 cm^{-1} due to matrix embedding. A bulk matrix value to compare with is not available. In CCl_4 , the main band is observed at $3465\text{--}3466\text{ cm}^{-1}$ [13,17], thus quantifying the solvent shift at 32 cm^{-1} . A second band was observed at $3479\text{--}3482\text{ cm}^{-1}$ and might correspond to the second (anti) isomer mentioned above [17,14].

A single strong dimer band appears in the He jet spectra at 3324 cm^{-1} , in agreement with the theoretical predictions. The experimental red shift thus amounts to 173 cm^{-1} , in fortuitously close agreement to the harmonic B3LYP predictions of $164\text{--}188\text{ cm}^{-1}$ (Tab. 8). The MP2 prediction of 126 cm^{-1} would require atypically large anharmonicity contributions to be reconciled with experi-

ment. It will be interesting to see what much higher level approximations predict for this wavenumber shift. Note that the strength of the experimental dimer band is consistent with somewhat less than 5% dimer fraction in the jet. No signs of a dimerization-induced Fermi resonance with bending modes [43] can be detected. The shift upon Ar embedding (lowest trace of Fig. 14) is slightly larger than in the monomer and shows that the Ar nanomatrix [44] interacts differently with the monomer and the dimer. Comparison of the cold dimer shift to thermally excited dimers in room temperature solutions is only of limited value [45], because the hydrogen bond is significantly attenuated at 300 K and competes with solvent interactions [23]. In CCl_4 solution, a hydrogen bond-induced red shift of $147\text{--}149\text{ cm}^{-1}$ was found [14,17]. Comparison with the dimerization red-shift of pyrrole-2-carboxaldehyde (220 cm^{-1} for the N-H stretching mode [18]) shows that the aldehyde C=O is a better acceptor than the ester C=O.

In the jet spectra, no evidence for π stacking or pyrrole-like N-H $\cdots\pi$ aggregation can be found [46,47]. This provides clear experimental evidence for the dominance of N-H \cdots O=C interactions over $\pi\cdots\pi$ [25] and N-H $\cdots\pi$ [47] contacts in this case, although the latter come quite close to regular hydrogen bond interactions.

Fig. 15 shows the C=O stretching range. The dominant gas phase band collapses to a narrow jet monomer absorption at 1732 cm^{-1} due to the reduction in the rotational temperature. This may be compared to the CCl_4 solution value of 1701 cm^{-1} , i.e. the C=O band experiences a similar solvent shift as the N-H band. However, this refers to the dominant band, only. In CCl_4 solution, there is actually a quartet of bands [13]. Two of them are probably related to aggregates, but a 18 cm^{-1} blue-shifted band persists at high dilution [14]. It was assigned to the metastable (anti) monomer of MPC and may find its correspondence in a weak gas phase feature at 1757 cm^{-1} . In the jet spectrum, the signal-to-noise ratio is not sufficient to identify this band with certainty. This is also true for the C=O stretching band of the dimer, which is expected at lower wavenumber. Improved spectra could be obtained by using heated nozzles [40], as the thermal stability of MPC appears to be sufficiently high. A red-shift of 12 cm^{-1} [13] (or 25 cm^{-1} [15]) observed in CCl_4 -solution may be considered to represent a lower limit for the expected jet-cooled red-shift. In any case, the jet spectrum does not provide any evidence for the Fermi resonance invoked in an earlier study [17].

In summary, there is a single dominant monomer conformation in MPC which aggregates into a single planar dimer, when expanded in a supersonic jet at high dilution. The spectra are well described at B3LYP level, which predicts a second monomer conformation at the detection limit of the current setup. The strongly red-shifted single band of the dimer provides a clear signature of strong, symmetric hydrogen bonding, not unlike the situation in antiparallel peptide β -sheets [48,18].

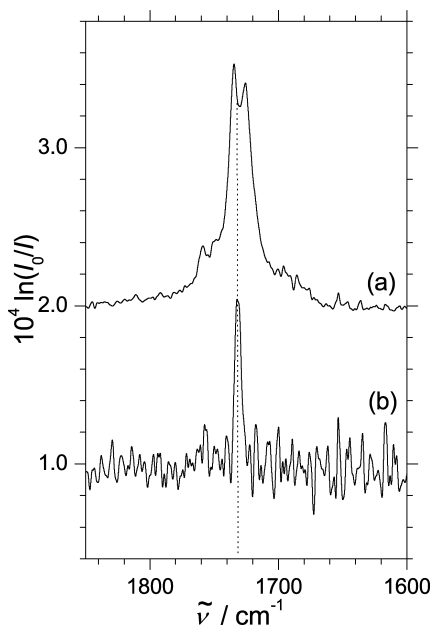


Fig. 15. C=O stretching region of the IR spectrum of methyl 1H-pyrrole-2-carboxylate. (a) Gas phase after 10-fold intensity compression. (b) Jet spectrum of $\leq 0.003\%$ MPC in He at 0.7 bar.

4. Conclusions

Two structurally similar compounds involving N-H and C=O functional groups have been investigated by supersonic jet spectroscopy and are shown to differ substantially in their aggregation patterns. Proline esters exhibit conformational flexibility and unspecific hydrogen bond patterns, whereas pyrrole esters as their dehydrogenated homologs form strongly bound planar dimers.

Proline esters show a subtle conformational isomerism due to different puckering forms of the pyrrolidine ring. We could correlate the most stable isomer with the lower frequency NH stretching band. It would be interesting to confirm its proposed structure by microwave spectroscopy [49].

As the proline esters are chiral, differences between homo- and heteroconfigurational dimers might be expected. Our inability to identify clean experimental signatures of chirality recognition contrasts recent findings for proline itself, when it aggregates to charged nanometer-scale assemblies in electrospray sources [50]. This is no contradiction, because the intermolecular forces in (charged) proline clusters are more pronounced and more directed than those of the proline ester clusters studied in the present work. Furthermore, the weak dimerization propensity makes chirality recognition difficult to detect in proline esters and we find at least circumstantial evidence that it may be present in trimers. It is con-

ceivable that larger aggregates show more pronounced chirality recognition effects, but they are difficult to study due to the instability of the esters.

In the case of pyrrole carboxylates with their peptide-like N-H bond, aggregation leads to symmetrical dimers, whose hydrogen bond strength approaches that in carboxylic dimers. Like the related pyrrole carboxaldehydes [18], they may serve as elementary β -sheet forming peptide models.

In terms of an adequate quantum-chemical treatment, the two systems are also quite disparate. Intermolecular interactions in proline esters involve subtle hydrogen bonds and dispersion interactions, for which hybrid density functionals such as the B3LYP approach are inappropriate. Hence, MP2 is probably the lowest level for which qualitatively correct results can be expected. In contrast, this method fails for the analogous aromatic compound MPC, at least for moderately large standard basis sets. Presumably, this is related to the aromatic character of the N-H bond. Because the hydrogen bonding is strong, B3LYP provides an acceptable description of the aggregation behavior for this compound. The two systems discussed in this work can thus contribute to a reliable assessment of the performance of density functional methods in the weak to strong hydrogen bond regime [51].

Beyond the proline case, the two model systems mimic the influence of N-terminal acetylation of peptides on intermolecular aggregation. The profound differences in aggregation tendency may be one of the reasons why nature employs this modification of the peptide N $^{\alpha}$ -terminus so frequently [52].

Our findings underscore the need for detailed tests of quantum chemical approaches on realistic model systems, before they can be trusted in more complex situations. The switch from sp^3 to sp^2 hybridization of the N-H bond leads into a completely different regime of intermolecular interactions with rather different demands on the level of theoretical modelling.

Acknowledgement

We thank C. Rice for substantial advice in the early phase of this project and Thorsten Stafforst and Nina Tölle for support in the synthesis of the proline esters. We gratefully acknowledge computational resources from the GWDG and financial support by the Deutsche Forschungsgemeinschaft via GRK 782 (www.pcg.de) as well as by the Fonds der Chemischen Industrie.

References

1. M. Roehrig and H. G. Wagner, *Ber. Bunsenges. Phys. Chem.* **98** (1994) 858–863.
2. W. Hack, H. G. Wagner, and A. Zasytkin, *Ber. Bunsenges. Phys. Chem.* **98** (1994) 156–164.
3. Dieter Seebach, Albert K. Beck, and Daniel J. Bierbaum, *Chem. & Biodivers.* **1** (2004) 1111–1239.
4. M. Gerhards and C. Unterberg, *Phys. Chem. Chem. Phys.* **4** (2002) 1760–1765.

5. I. Hünig, K. A. Seefeld, and K. Kleinermanns, *Chem. Phys. Lett.* **369** (2003) 173–179.
6. Anthi Kamariotis, Oleg V. Boyarkin, Sebastien R. Mercier, Rainer D. Beck, Matthew F. Bush, Evan R. Williams, and Thomas R. Rizzo, *J. Am. Chem. Soc.* **128** (2006) 905–916.
7. Thomas Häber, Ulrich Schmitt, and Martin A. Suhm, *Phys. Chem. Chem. Phys.* **1** (1999) 5573–5582.
8. Rolf Linder, Michael Nispel, Thomas Häber, and Karl Kleinermanns, *Chem. Phys. Lett.* **409** (2005) 260–264.
9. Eszter Czinki and Attila G. Császár, *Chem. Eur. J.* **9** (2003) 1008–1019.
10. Pinak Chakrabarti and Sarmistha Chakrabarti, *J. Mol. Biol.* **284** (1998) 867–873.
11. Santanu Mukherjee, Jung Woon Yang, Sebastian Hoffmann, and Benjamin List, *Chem. Rev.* **107** (2007) 5471–5569.
12. R. Alan Jones and A. G. Moritz, *Spectrochim. Acta* **21** (1965) 295–299.
13. Alina T. Dubis and Sławomir J. Grabowski, *J. Phys. Chem. A* **107** (2003) 8723–8729.
14. Alina T. Dubis and Sławomir J. Grabowski, *J. Mol. Struct.* **562** (2001) 107–117.
15. Alina T. Dubis and Sławomir J. Grabowski, *New J. Chem.* **26** (2002) 165–169.
16. Zhenming Yin and Zucheng Li, *Tetrahedron Lett.* **47** (2006) 7875–7879.
17. Perry T. Kaye, Robert Macrae, G. Denis Meakins, and Colin H. Patterson, *J. Chem. Soc., Perkin Trans. 2* (1980) 1631–1635.
18. Corey A. Rice, Ingo Dauster, and Martin A. Suhm, *Phys. Chem. Chem. Phys.* **126** (2007) 134313.
19. Richard L. Elliott, Hana Kopecka, Nan-Horng Lin, Yun He, and David S. Garvey, *Synthesis* (1995) 772–774.
20. Hans-Jürgen Federsel, Erik Könberg, Lars Lilljequist, and Britt-Marie Swahn, *J. Org. Chem.* **55** (1990) 2254–2256.
21. Aude Simon, Luke MacAleese, Philippe Maître, Joël Lemaire, and Terrance B. McMahon, *J. Am. Chem. Soc.* **129** (2007) 2829–2840.
22. Nicole Borho, Martin A. Suhm, Katia Le Barbu-Debus, and Anne Zehnacker, *Phys. Chem. Chem. Phys.* **8** (2006) 4449–4460.
23. Adam Allerhand and Paul von R. Schleyer, *J. Am. Chem. Soc.* **85** (1963) 371–380.
24. M. Gerhards, C. Unterberg, and A. Gerlach, *Phys. Chem. Chem. Phys.* **4** (2002) 5563–5565.
25. Rafal A. Bachorz, Florian A. Bischoff, Sebastian Höfener, Wim Klopper, Philipp Ottiger, Roman Leist, Jann A. Frey, and Samuel Leutwyler, *Phys. Chem. Chem. Phys.* **10** (2008) 2758–2766.
26. T. Scharge, D. Luckhaus, and M. A. Suhm, *Chem. Phys.* **346** (2008) 167–175.
27. Anne Zehnacker and Martin A. Suhm, *Angew. Chem., Int. Ed.* **47** (2008) 6970–6992.
28. Nicole Borho and Martin A. Suhm, *Org. Biomol. Chem.* **1** (2003) 4351–4358.
29. S. G. Stepanian, I. D. Reva, E. D. Radchenko, and L. Adamowicz, *J. Phys. Chem.* **105** (2001) 10664–10672.
30. M. J. Frisch, G. W. Trucks, H. B. Schlegel, G. E. Scuseria, M. A. Robb, J. R. Cheeseman, J. A. Montgomery, Jr., T. Vreven, K. N. Kudin, J. C. Burant, J. M. Millam, S. S. Iyengar, J. Tomasi, V. Barone, B. Mennucci, M. Cossi, G. Scalmani, N. Rega, G. A. Petersson, H. Nakatsuji, M. Hada, M. Ehara, K. Toyota, R. Fukuda, J. Hasegawa, M. Ishida, T. Nakajima, Y. Honda, O. Kitao, H. Nakai, M. Klene, X. Li, J. E. Knox, H. P. Hratchian, J. B. Cross, C. Adamo, J. Jaramillo, R. Gomperts, R. E. Stratmann, O. Yazyev, A. J. Austin, R. Cammi, C. Pomelli, J. W. Ochterski, P. Y. Ayala, K. Morokuma, G. A. Voth, P. Salvador, J. J. Dannenberg, V. G. Zakrzewski, S. Dapprich, A. D. Daniels, M. C. Strain, O. Farkas, D. K. Malick, A. D. Rabuck, K. Raghavachari, J. B. Foresman, J. V. Ortiz, Q. Cui, A. G. Baboul, S.

- Clifford, J. Cioslowski, B. B. Stefanov, G. Liu, A. Liashenko, P. Piskorz, I. Komaromi, R. L. Martin, D. J. Fox, T. Keith, M. A. Al-Laham, C. Y. Peng, A. Nanayakkara, M. Challacombe, P. M. W. Gill, B. Johnson, W. Chen, M. W. Wong, C. Gonzalez, and J. A. Pople, Gaussian03, Revisions B.04 and C.02. Gaussian Inc., Pittsburgh PA (2003).
31. L. Carballeira, I. Pérez-Juste, and C. Van Alsenoy, *J. Phys. Chem. A* **106** (2002) 3873–3884.
 32. R. Balasubramanian, A. V. Lakshminarayanan, M. N. Sabesan, G. Tegoni, K. Venkatesan, and G. N. Ramachandran, *International Journal of Protein Research III* (1971) 25–33.
 33. Magdalena Pecul, Kenneth Ruud, Antonio Rizzo, and Trygve Helgaker, *J. Phys. Chem. A* **108** (2004) 4269–4276.
 34. H. Ripperger and K. Schreiber, *Journal für Praktische Chemie* **313** (1971) 825–838.
 35. Lin Guoqiang, Mats Hjalmarsson, Hans-Erik Högberg, Karen Jernstedt, and Torbjörn Norin, *Acta Chemica Scandinavica B* **38** (1984) 795–801.
 36. A. A. Prishchenko, M. V. Livantsov, D. A. Pisarnitskii, and V. S. Petrosyan, *Zhurnal Obshchei Khimii* **63** (1993) 2020–2025.
 37. P. Pratesi, L. Arpesella, and A. La Manna, *J. Am. Chem. Soc.* **75** (1953) 5476–5478.
 38. George W. Anderson and Francis M. Callahan, *J. Am. Chem. Soc.* **82** (1960) 3359–3363.
 39. Thomas B. Adler, Nicole Borho, Markus Reiher, and Martin A. Suhm, *Angew. Chem., Int. Ed.* **45** (2006) 3440–3445.
 40. Merwe Albrecht, Corey A. Rice, and Martin A. Suhm, *J. Phys. Chem. A* **112** (2008) 7530–7542.
 41. Corinna Emmeluth and Martin A. Suhm, *Phys. Chem. Chem. Phys.* **5** (2003) 3094–3099.
 42. Alina T. Dubis and Sławomir J. Grabowski, *Spectrochim. Acta Part A* **58** (2002) 213–215.
 43. T. N. Wassermann, C. A. Rice, M. A. Suhm, and D. Luckhaus, *J. Chem. Phys.* **127** (2007) 234309.
 44. Tobias N. Wassermann, Philipp Zielke, Juhyon J. Lee, Christine Cézard, and Martin A. Suhm, *J. Phys. Chem. A* **111** (2007) 7437–7448.
 45. Merwe Albrecht, Philipp Zielke, Corey A. Rice, and Martin A. Suhm, *J. Mol. Struct.* **880** (2008) 2–13.
 46. Yoshiteru Matsumoto and Kenji Honma, *J. Chem. Phys.* **127** (2007) 184310.
 47. Ingo Dauster, Corey A. Rice, Philipp Zielke, and Martin A. Suhm, *Phys. Chem. Chem. Phys.* **10** (2008) 2827–2835.
 48. H. Fricke, A. Gerlach, and M. Gerhards, *Phys. Chem. Chem. Phys.* **8** (2006) 1660–1662.
 49. David F. Plusquellic, Isabelle Kleiner, Jean Demaison, Richard D. Suenram, Richard J. Lavrich, Frank J. Lovas, Gerald T. Fraser, and Vadim V. Ilyushin, *J. Chem. Phys.* **125** (2005) 104312.
 50. Sunnie Myung, Marco Fioroni, Ryan R. Julian, and Stormy L. Koeniger, *J. Am. Chem. Soc.* **128** (2006) 10833–10839.
 51. E. R. Johnson and G. A. DiLabio, *Chem. Phys. Lett.* **419** (2006) 333–339.
 52. Bogdan Polevoda and Fred Sherman, *J. Biol. Chem.* **275** (2000) 36479–36482.